

The Higgs sector of the phenomenological MSSM in the light of the Higgs boson discovery

A. Arbey^{a,b,c}, M. Battaglia^{c,d,e}, A. Djouadi^{c,f} and F. Mahmoudi^{c,g}

^a Université de Lyon, France; Université Lyon 1, CNRS/IN2P3, UMR5822 IPNL,
F-69622 Villeurbanne Cedex, France.

^b Centre de Recherche Astrophysique de Lyon, Observatoire de Lyon, Saint-Genis Laval Cedex,
F-69561, France; CNRS, UMR 5574; Ecole Normale Supérieure de Lyon, Lyon, France.

^c CERN, CH-1211 Geneva 23, Switzerland.

^d Santa Cruz Institute of Particle Physics, University of California, Santa Cruz, CA 95064, USA.

^e Lawrence Berkeley National Laboratory, Berkeley, CA 94720, USA.

^f Laboratoire de Physique Théorique, Université Paris XI and CNRS, F-91405 Orsay, France.

^g Clermont Université, Université Blaise Pascal, CNRS/IN2P3,
LPC, BP 10448, 63000 Clermont-Ferrand, France.

Abstract

The long awaited discovery of a new light scalar boson at the LHC opens up a new era of studies of the Higgs sector in the Standard Model and in its extensions. In this paper we discuss the consequences of the observation of a light Higgs boson with the mass and rates reported by the ATLAS and CMS collaborations on the parameter space of the phenomenological MSSM, including also the LHC searches for heavier Higgs bosons and supersymmetric particle partners, as well as the constraints from B -physics and dark matter. We explore the various regimes of the MSSM Higgs sector depending on the parameters M_A and $\tan \beta$ and show that only two of them are still allowed by all present experimental constraints: the decoupling regime in which there is only one light and standard-like Higgs boson while the heavier Higgs states decouple from gauge bosons, and the supersymmetric regime, in which there are light supersymmetric particle partners which might affect the decay properties of the light Higgs boson, in particular its di-photon and invisible decays.

1 Introduction

Results of the search for the Higgs bosons at the LHC with the 10 fb^{-1} data collected in 2011 at 7 TeV and 2012 at 8 TeV have just been presented by the ATLAS [1] and CMS [2] collaborations and there is now a 5σ evidence by each of the experiments for a new particle with a mass of $\approx 126 \text{ GeV}$. Complementary evidence is also provided by the updated combination of the Higgs searches performed by the CDF and D0 collaborations at the Tevatron [3], which has also been just released. As we are entering an era of Higgs studies, these results have deep implications for the Minimal Supersymmetric Standard Model (MSSM). The implications of a Higgs boson with a mass value around 126 GeV in the context of Supersymmetry have been already widely discussed [4–7] since the first evidence of a signal at the LHC was presented at the end of 2011. In particular, we have discussed the consequences of the value of M_h for the unconstrained phenomenological MSSM (pMSSM) with 22 free parameters [8], for constrained MSSM scenarios such as the minimal gravity, gauge and anomaly mediated SUSY-breaking models, and in scenarios in which the supersymmetric spectrum is extremely heavy [4]. We have shown that only when the SUSY-breaking scale is very large or the mixing in the stop sector is significant the observed M_h value can be accommodated in these models. This disfavors many constrained scenarios such as the minimal anomaly and gauge mediated SUSY-breaking models and some (even more constrained) versions of the minimal super-gravity model.

In this paper, we extend the previous study in new directions afforded by the improved data from the LHC experiments. First, we refine our analysis of the implications of the value $M_h \approx 126 \text{ GeV}$ for the decoupling regime by considering different types of stop mixing scenarios which significantly affect the maximal mass value and we explore the implications of a broader range of the top quark mass value, $m_t = (173 \pm 3) \text{ GeV}$, on M_h . Then, we analyse in detail the implications of the ATLAS and CMS searches for the heavier MSSM Higgs bosons, the CP-even H , a pseudoscalar A and two charged H^\pm states. In particular, we discuss the $A/H/h \rightarrow \tau^+\tau^-$ for the neutral and the $t \rightarrow bH^+ \rightarrow b\tau\nu$ searches for the charged states to further constrain the $[M_A, \tan\beta]$ parameter space, where $\tan\beta$ is the ratio of the vacuum expectation values of the two Higgs doublet fields. We also discuss the effect of the recent LHCb results for the decay $B_s \rightarrow \mu^+\mu^-$ on the Higgs sector, as well as the super-particle LHC searches and the dark matter constraints. Most importantly, we study other regimes than the decoupling regime of the pMSSM: the anti-decoupling regime for low M_A in which the roles of the h and H bosons are reversed, the intense coupling regime in which the three neutral particles h, A, H are rather close in mass, the intermediate regime at relatively low $\tan\beta$ in which the couplings of H, A to gauge+Higgs bosons are not too suppressed and the vanishing coupling regime in which the coupling of the h state to bottom quarks or gauge bosons is suppressed. Using the latest ATLAS, CMS and Tevatron data, we show that all these scenarios are now almost ruled out. Finally, we start studying the implications of the rates reported by the LHC experiments in the $\gamma\gamma$ and ZZ final states used to obtain the Higgs boson signal and we comment on the $b\bar{b}$ final state to which the Tevatron is most sensitive. We perform a full scan of the pMSSM parameter space in order to delineate the regions which fit best the experimental data, including a possible enhancement of the $h \rightarrow \gamma\gamma$ rate.

The paper is organised as follows. First, we briefly describe the pMSSM and its Higgs sector with its various regimes and summarise the Higgs decays and the production cross sections at the LHC. In section 3, we present the analysis of these different Higgs regimes

and the implications on the pMSSM parameters in the light of the LHC Higgs discovery and constraints. Section 4 has a short conclusion.

2 The theoretical set-up

2.1 The pMSSM Higgs sector

In the MSSM the Higgs sector is extended to contain five Higgs particles ¹. The lightest h boson has in general the properties of the Standard Model (SM) Higgs boson ² and is expected to have a mass $M_h \lesssim 115\text{--}135$ GeV depending on the MSSM parameters, in particular, the ratio $\tan\beta$ of the vacuum expectation values of the two Higgs doublet fields that break the electro-weak symmetry in the MSSM.

By virtue of supersymmetry, only two parameters are needed to describe the Higgs sector at tree-level. These can be conveniently chosen to be the pseudoscalar boson mass M_A and the ratio of vacuum expectation values of the two Higgs fields that break the symmetry, $\tan\beta = v_2/v_1$. However, accounting for the radiative corrections to the Higgs sector, known to play an extremely important role [10], all soft SUSY-breaking parameters which are of $\mathcal{O}(100)$ in addition to those of the SM, become relevant. This makes any phenomenological analysis in the most general MSSM a very complicated task. A phenomenologically more viable MSSM framework, the pMSSM, is defined by adopting the following assumptions: *i*) all soft SUSY-breaking parameters are real and there is no new source of CP-violation; *ii*) the matrices for the sfermion masses and for the trilinear couplings are all diagonal, implying no flavor change at tree-level; and *iii*) the soft SUSY-breaking masses and trilinear couplings of the first and second sfermion generations are the same at the electro-weak symmetry breaking scale. Making these three assumptions will lead to only 22 input parameters in the pMSSM:

- $\tan\beta$: the ratio of the vevs is expected to lie in the range $1 \lesssim \tan\beta \lesssim m_t/m_b$;
- M_A : the pseudoscalar Higgs mass that ranges from M_Z to the SUSY-breaking scale;
- μ : the Higgs–higgsino (supersymmetric) mass parameter (with both signs);
- M_1, M_2, M_3 : the bino, wino and gluino mass parameters;
- $m_{\tilde{q}}, m_{\tilde{u}_R}, m_{\tilde{d}_R}, m_{\tilde{l}}, m_{\tilde{e}_R}$: the first/second generation sfermion mass parameters;
- A_u, A_d, A_e : the first/second generation trilinear couplings;
- $m_{\tilde{Q}}, m_{\tilde{t}_R}, m_{\tilde{b}_R}, m_{\tilde{L}}, m_{\tilde{\tau}_R}$: the third generation sfermion mass parameters;
- A_t, A_b, A_τ : the third generation trilinear couplings.

Such a model has more predictability and it offers an adequate framework for phenomenological studies. In general, only a small subset of the parameters appears when looking at a given sector of the pMSSM, such as the Higgs sector in this case. Some of these parameters will enter the radiative corrections to the Higgs boson masses and couplings. At the one-loop level, the h boson mass receives corrections that grow as the fourth power of the top quark mass m_t (we use the running $\overline{\text{MS}}$ mass to re-sum some higher order corrections) and logarithmically

¹ For a review of the MSSM Higgs sector [9]. For reviews on the radiative corrections in the MSSM Higgs sector and a complete set of references, see [10]

²For a review of the SM Higgs boson, see [11]

with the SUSY-breaking scale or common squark mass M_S ; the trilinear coupling in the stop sector A_t plays also an important role. The leading part of these corrections reads [12]

$$\epsilon = \frac{3\bar{m}_t^4}{2\pi^2 v^2 \sin^2 \beta} \left[\log \frac{M_S^2}{\bar{m}_t^2} + \frac{X_t^2}{2M_S^2} \left(1 - \frac{X_t^2}{6M_S^2} \right) \right]. \quad (1)$$

We have defined the SUSY-breaking scale M_S to be the geometric average of the two stop masses (that we take $\lesssim 3$ TeV not to introduce excessive fine-tuning)

$$M_S = \sqrt{m_{\tilde{t}_1} m_{\tilde{t}_2}} \quad (2)$$

and introduced the mixing parameter X_t in the stop sector (that we assume $\lesssim 3M_S$),

$$X_t = A_t - \mu \cot \beta. \quad (3)$$

The radiative corrections have a much larger impact and maximise the h boson mass in the so-called “maximal mixing” scenario, where the trilinear stop coupling in the $\overline{\text{DR}}$ scheme is

$$\text{maximal mixing scenario : } X_t = \sqrt{6} M_S. \quad (4)$$

In turn, the radiative corrections are much smaller for small values of X_t , i.e. in the

$$\text{no mixing scenario : } X_t = 0. \quad (5)$$

An intermediate scenario is when X_t is of the same order as M_S which is sometimes called the

$$\text{typical mixing scenario : } X_t = M_S. \quad (6)$$

These mixing scenarios have been very often used as benchmarks for the analysis of MSSM Higgs phenomenology [13]. The maximal mixing scenario has been particularly privileged since it gives a reasonable estimate of the upper bound on the h boson mass, M_h^{max} . We will discuss these scenarios but, compared to the work of Ref. [13], we choose here to vary the scale M_S . Together with the requirements on X_t in eqs. (4–6), we adopt the following values for the parameters entering the pMSSM Higgs sector,

$$A_t = A_b, \quad M_2 \simeq 2 M_1 = |\mu| = \frac{1}{5} M_S, \quad M_3 = 0.8 M_S, \quad (7)$$

and vary the basic inputs $\tan \beta$ and M_A . For the values $\tan \beta = 60$ and $M_A = M_S = 3$ TeV and a top quark pole of mass of $m_t = 173$ GeV, we would obtain a maximal Higgs mass value $M_h^{\text{max}} \approx 135$ GeV for maximal mixing once the full set of known radiative corrections up to two loops is implemented [14]. In the no-mixing and typical mixing scenarios, one obtains much smaller values, $M_h^{\text{max}} \approx 120$ GeV and $M_h^{\text{max}} \approx 125$ GeV, respectively. Scanning over the soft SUSY-breaking parameters, one may increase these M_h^{max} values by up to a few GeV.

It is important to note that the dominant two-loop corrections have been calculated in the $\overline{\text{DR}}$ scheme [15] and implemented in the codes **Suspect** [16] and **SOFTSUSY** [17] that we will use here for the MSSM spectrum, but also in the on-shell scheme [18] as implemented in **FeynHiggs** [19]. In general, the results for M_h in the two scheme differ by at most 2 GeV, which we take as a measure of the missing higher order effects. Quite recently, the dominant three-loop contribution to M_h has been calculated and found to be below 1 GeV [20]. Thus, the mass of the lightest h boson can be predicted with an accuracy of $\Delta M_h \sim 3$ GeV and this is the theoretical uncertainty on M_h that we assume.

2.2 The various regimes of the pMSSM

The spectrum in the various regimes of the pMSSM Higgs sector [9], depends on the values of M_A and also on $\tan\beta$, and that we will confront to the latest LHC and Tevatron data in this paper.

We start from the decoupling regime [21] that has been already mentioned and which in principle occurs for large values of M_A but is reached in practice at $M_A \gtrsim 300$ GeV for low $\tan\beta$ values and already at $M_A \gtrsim M_h^{\max}$ for $\tan\beta \gtrsim 10$. In this case, the CP-even h boson reaches its maximal mass value M_h^{\max} and its couplings to fermions and gauge bosons (as well as its self-coupling) become SM-like. The heavier H boson has approximately the same mass as the A boson and its interactions are similar, i.e. its couplings to gauge bosons almost vanish and the couplings to bottom (top) quarks and τ leptons fermions are (inversely) proportional to $\tan\beta$. Hence, one will have a SM-like Higgs boson $h \equiv H_{\text{SM}}$ and two pseudo-scalar (like) Higgs particles, $\Phi = H, A$. The H^\pm boson is also degenerate in mass with the A boson and the intensity of its couplings to fermions is similar. Hence, in the decoupling limit, the heavier $H/A/H^\pm$ bosons almost decouple and the MSSM Higgs sector reduces effectively to the SM Higgs sector, but with a light h boson.

The anti-decoupling regime [22] occurs for a light pseudo-scalar Higgs boson, $M_A \lesssim M_h^{\max}$, and is exactly opposite to the decoupling regime. The roles of the h and H bosons are reversed and at large $\tan\beta$ values, the h boson is degenerate in mass with the pseudo-scalar A , $M_h \simeq M_A$, while the H boson has a mass close to its minimum which is in fact M_h^{\max} . Because of the upper bound on M_h , all Higgs particles are light. Here, it is the h boson which has couplings close to those of A , $\Phi = h, A$, while the H boson couplings are SM-like, $H \equiv H_{\text{SM}}$.

The intense-coupling regime [23] occurs when the mass of the pseudo-scalar A boson is close to M_h^{\max} . In this case, the three neutral Higgs bosons h, H and A (as well as the charged Higgs particles) have comparable masses, $M_h \sim M_H \sim M_A \sim M_h^{\max}$. The mass degeneracy is more effective when $\tan\beta$ is large. Here, both the h and H bosons have still enhanced couplings to b -quarks and τ leptons and suppressed couplings to gauge bosons and top quarks, as is the pseudo-scalar A . Hence, one approximately has three pseudo-scalar like Higgs particles, $\Phi \equiv h, H, A$ with mass differences of the order of 10–20 GeV.

The intermediate-coupling regime occurs for low values of $\tan\beta$, $\tan\beta \lesssim 5$ –10, and a not too heavy pseudo-scalar Higgs boson, $M_A \lesssim 300$ –500 GeV [9]. Hence, we are not yet in the decoupling regime and both CP-even Higgs bosons have non-zero couplings to gauge bosons and their couplings to down-type (up-type) fermions (as is the case for the pseudoscalar A boson) are not strongly enhanced (suppressed) since $\tan\beta$ is not too large. This scenario is already challenged by LEP2 data which call for moderately large values of $\tan\beta$.

The vanishing-coupling regime occurs for relatively large values of $\tan\beta$ and intermediate to large M_A values, as well as for specific values of the other MSSM parameters. The latter parameters, when entering the radiative corrections, could lead to a strong suppression of the couplings of one of the CP-even Higgs bosons to fermions or gauge bosons, as a result of the cancellation between tree-level terms and radiative corrections [24]. An example of such a situation is the small α_{eff} scenario which has been used as a benchmark [13] and in which the Higgs to $b\bar{b}$ coupling is strongly suppressed.

Within the plane $[M_A, \tan\beta]$, the parameter space in which the above regimes of the pMSSM

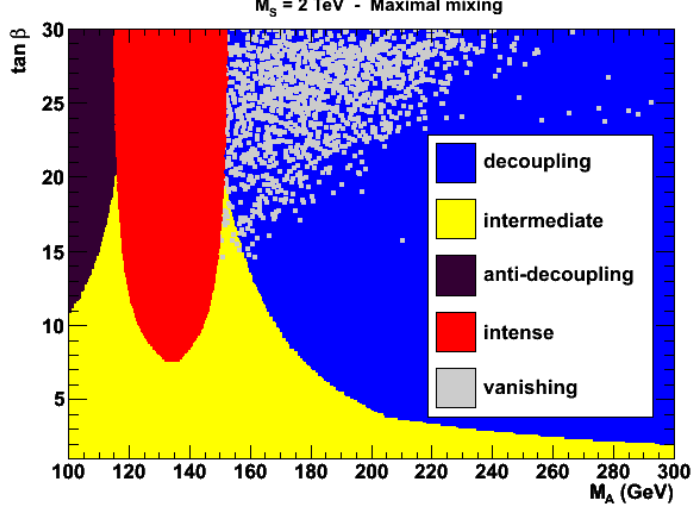


Figure 1: The parameter space for the various regimes of the MSSM Higgs sector as defined in the text and in eq. (8) in the $[M_A, \tan \beta]$ plane; the maximal mixing scenario with $M_S = 2$ TeV is adopted.

Higgs sector occur are displayed in Figure 1. We have chosen the usual maximal mixing scenario with $M_S = 2$ TeV and the other SUSY parameters as in eq. (7), except for the vanishing coupling scenario, where we have scanned over the SUSY parameters, and only $\approx 5 \times 10^{-4}$ of the scanned points fulfil its requirements. The following conditions have been imposed:

$$\begin{aligned}
\text{decoupling regime} & : \cos^2(\beta - \alpha) \leq 0.05 \\
\text{anti-decoupling regime} & : \cos^2(\beta - \alpha) \geq 0.95 \\
\text{intermediate-coupling regime} & : 0.05 \leq \cos^2(\beta - \alpha) \leq 0.7, \quad \tan \beta \leq 10 \\
\text{intense-coupling regime} & : M_A \lesssim 140 \text{ GeV}, \quad g_{hbb}^2 \text{ and } g_{Hbb}^2 \geq 50 \\
\text{vanishing-coupling regime} & : M_A \gtrsim 200 \text{ GeV}, \quad g_{hbb}^2 \text{ or } g_{hVV}^2 \leq 0.05.
\end{aligned} \tag{8}$$

In addition, we have to consider the SUSY regime, in which some SUSY particles such as the charginos, neutralinos as well as the third generation sleptons and squarks, could be light enough to significantly affect the phenomenology of the MSSM Higgs bosons. For instance, light particles could substantially contribute to the loop induced production and decays modes of the lighter h boson [25, 26] and could even appear (in the case of the lightest neutralino) in its decay product as will be discussed below.

2.3 Higgs decays and production in the pMSSM

For the relatively large values of $\tan \beta$ presently probed at the LHC, $\tan \beta \gtrsim 7$ as discussed below, the couplings of the non-SM like Higgs bosons to b quarks and τ leptons are so strongly enhanced and those to top quarks and gauge bosons suppressed, that the pattern becomes as simple as the following (more details can be found in Ref. [9]):

- The $\Phi = A$ or H/h bosons in the decoupling/anti-decoupling limit decay almost exclusively into $b\bar{b}$ and $\tau^+\tau^-$ pairs, with branching ratios of, respectively, $\approx 90\%$ and $\approx 10\%$, and all other channels are suppressed to a level where their branching ratios are negligible.

- The H^\pm particles decay into fermion pairs: mainly $H^+ \rightarrow t\bar{b}$ and $H^+ \rightarrow \tau\nu_\tau$ final states for H^\pm masses, respectively, above and below the $t\bar{b}$ threshold.

- The CP-even h or H boson, depending on whether we are in the decoupling or anti-decoupling regime, will have the same decays as the SM Higgs boson. For $M_{h/H} \approx 126$ GeV, the main decay mode will be the $b\bar{b}$ channel with a $\sim 60\%$ probability, followed by the decays into $c\bar{c}$, $\tau^+\tau^-$ and the loop induced decay into gluons with $\sim 5\%$ branching ratios. The WW^* decay reaches the level of 20%, while the rate for ZZ^* is a few times 10^{-2} . The important loop induced $\gamma\gamma$ decay mode which leads to clear signals at the LHC have rates of $\mathcal{O}(10^{-3})$.

In the intense-coupling regime, the couplings of both h and H to gauge bosons and up-type fermions are suppressed and those to down-type fermions are enhanced. The branching ratios of the h and H bosons to $b\bar{b}$ and $\tau^+\tau^-$ final states are thus the dominant ones, with values as in the case of the pseudoscalar A boson. In the intermediate-coupling regime, interesting decays of H , A and H^\pm into gauge and/or Higgs bosons occur, as well as $A/H \rightarrow t\bar{t}$ decays, but they are suppressed in general. Finally, for the rare vanishing-coupling regime when the Higgs couplings to b -quarks and eventually τ -leptons accidentally vanish, the outcome is spectacular for the h boson: the WW^* mode becomes dominant and followed by $h \rightarrow gg$, while the interesting $h \rightarrow \gamma\gamma$ and $h \rightarrow ZZ^*$ decay modes are enhanced.

In the case of the SM-like Higgs particle (that we assume now to be the h boson), there are two interesting scenarios which might make its decays rather different. First we have the scenario with the Higgs bosons decaying into supersymmetric particles. Because most sparticles must be heavier than about 100 GeV, there is no SUSY decays of the h boson except for the invisible channel into a pair of the lightest neutralinos, $h \rightarrow \chi_1^0\chi_1^0$. This is particularly true when the gaugino mass universality relation $M_2 \sim 2M_1$ is relaxed, leading to light χ_1^0 states while the LEP2 bound, $m_{\chi_1^\pm} \gtrsim 100$ GeV, still holds. In the decoupling limit, the branching ratio of the invisible decay can reach the level of a few 10%. Decays of the heavier $A/H/H^\pm$ bosons, in particular into charginos, neutralinos, sleptons and top squarks, are in turn possible. However, for $\tan\beta \gtrsim 10$, they are strongly suppressed.

The second scenario of interest occurs when SUSY particles contribute to loop-induced Higgs decays. If scalar quarks are relatively light, they can lead to sizable contributions to the decays $h \rightarrow gg$ and $h \rightarrow \gamma\gamma$. Since scalar quarks have Higgs couplings that are not proportional to their masses, their contributions are damped by loop factors $1/m_Q^2$ and decouple from the vertices contrary to SM quarks. Only when $m_{\tilde{Q}}$ is not too large compared to M_h that the contributions are significant [25]. This is particularly true for the \tilde{t}_1 contributions to $h \rightarrow gg$, the reasons being that large X_t mixing leads to a \tilde{t}_1 that is much lighter than all other squarks and that the h coupling to stops involves a component which is proportional to $m_t X_t$ and, for large X_t , it can be strongly enhanced. Sbottom mixing, $\propto m_b X_b$, can also be sizable for large $\tan\beta$ and μ values and can lead to light \tilde{b}_1 states with strong couplings to the h boson. In $h \rightarrow \gamma\gamma$ decay, there are in addition slepton loops, in particular $\tilde{\tau}$ states which behave like scalar bottom quarks and have a strong mixing at high $\mu \tan\beta$, can make a large impact on the decay rate. Besides, chargino loops also enter the $h \rightarrow \gamma\gamma$ decay mode but their contribution is in general smaller since the Higgs- $\chi\chi$ couplings cannot be strongly enhanced.

For the evaluation of the decay branching ratios of the MSSM Higgs bosons, we use the program HDECAY [29], which incorporates all decay channels including those involving super-particles and the most important sets of higher order corrections and effects.

Coming to Higgs boson production at the LHC, for a SM-like particle H_{SM} there are essentially four mechanisms for single production [11]. These are gg fusion, $gg \rightarrow H_{\text{SM}}$, vector boson fusion, $qq \rightarrow H_{\text{SM}}qq$, Higgs-strahlung, $q\bar{q} \rightarrow H_{\text{SM}}V$ and $t\bar{t}$ associated Higgs production, $pp \rightarrow t\bar{t}H_{\text{SM}}$. The $gg \rightarrow H_{\text{SM}}$ process proceeds mainly through a heavy top quark loop and is by far the dominant production mechanism at the LHC. For a Higgs boson with a mass of ≈ 126 GeV, the cross section is more than one order of magnitude larger than in the other processes. Again for $M_{H_{\text{SM}}} \approx 126$ GeV, the most efficient detection channels are the clean but rare $H \rightarrow \gamma\gamma$ final states, the modes $H \rightarrow ZZ^* \rightarrow 4\ell^\pm$, $H \rightarrow WW^{(*)} \rightarrow \ell\ell\nu\nu$ with $\ell = e, \mu$ and, to a lesser extent, also $H_{\text{SM}} \rightarrow \tau^+\tau^-$. At the LHC and, most importantly, at the Tevatron one is also sensitive to $q\bar{q} \rightarrow H_{\text{SM}} + W/Z \rightarrow b\bar{b} + W/Z$ with $W \rightarrow \ell\nu$ and $Z \rightarrow \ell\ell, \nu\bar{\nu}$.

For the MSSM Higgs bosons, the above situation holds for the $h(H)$ state in the (anti-)decoupling regime. Since AVV couplings are absent, the A boson cannot be produced in Higgs-strahlung and vector boson fusion and the rate for $pp \rightarrow t\bar{t}A$ is strongly suppressed. For the $\Phi = A$ and $h(H)$ states, when we are in the (anti-)decoupling limit, the b quark will play an important role for large $\tan\beta$ values as the $\Phi b\bar{b}$ couplings are enhanced. One then has to take into account the b -loop contribution in the $gg \rightarrow \Phi$ processes which becomes the dominant component in the MSSM and consider associated Higgs production with $b\bar{b}$ final states, $pp \rightarrow b\bar{b} + \Phi$ which become the dominant channel in the MSSM. The latter process is in fact equivalent to $b\bar{b} \rightarrow \Phi$ where the b -quarks are taken from the proton in a five active flavor scheme. As the Φ bosons decay mainly into $b\bar{b}$ and $\tau^+\tau^-$ pairs, with the former being swamped by the QCD background, the most efficient detection channel would be $pp \rightarrow \Phi \rightarrow \tau^+\tau^-$. This process receives contributions from both the $gg \rightarrow \Phi$ and $b\bar{b} \rightarrow \Phi$ channels.

These processes also dominate the $h/H/A$ production in the intense coupling regime. In fact, in the three regimes above, when all processes leading to $\tau^+\tau^-$ final states are added up, the rate is $2 \times \sigma(gg + b\bar{b} \rightarrow A) \times \text{BR}(A \rightarrow \tau^+\tau^-)$. In the intermediate coupling regime, these process have very low cross sections as for $3-5 \leq \tan\beta \leq 7-10$, the $\Phi b\bar{b}$ couplings are not enough enhanced and the $\Phi t\bar{t}$ ones that control the gg fusion rate are still suppressed.

Finally, for the charged Higgs boson, the dominant channel is the production from top quark decays, $t \rightarrow H^\pm b$, for masses not too close to $M_{H^\pm} = m_t - m_b$. This is true in particular at low or large $\tan\beta$ values when the $t \rightarrow H^\pm b$ branching ratio is significant.

The previous discussion on MSSM Higgs production and detection at the LHC might be significantly altered if scalar quarks, in particular \tilde{t} and \tilde{b} , are light enough. Indeed, the Hgg and hgg vertices in the MSSM are mediated not only by the t/b loops but also by loops involving their partners similarly to the Higgs photonic decays. The $gg \rightarrow h$ cross section in the decoupling regime can be significantly altered by light stops and a strong mixing X_t which enhances the $h\tilde{t}_1\tilde{t}_1$ coupling. The cross section times branching ratio $\sigma(gg \rightarrow h) \times \text{BR}(h \rightarrow \gamma\gamma)$ for the lighter h boson at the LHC could be thus different from the SM case, even in the decoupling limit in which the h boson is supposed to be SM-like [25].

Finally, we should note that in the scenario in which the Higgs bosons, and in particular the lightest one h , decay into invisible lightest neutralinos, $h \rightarrow \chi_1^0\chi_1^0$, the observation of the final state will be challenging but possible at the LHC with a higher energy and more statistics. This scenario has recently been discussed in detail in Refs. [5, 30].

3 Analysis and results

3.1 pMSSM scans and software tools

The analysis is based on scans of the multi-parameter MSSM phase space. The input values of the electro-weak parameters, i.e. the top quark pole mass, the $\overline{\text{MS}}$ bottom quark mass, the electro-weak gauge boson masses, electromagnetic and strong coupling constants defined at the scale M_Z , are given below with their 1σ allowed ranges [32],

$$\begin{aligned} m_t &= (173 \pm 1) \text{ GeV}, \quad \bar{m}_b(\bar{m}_b) = (4.19^{+0.18}_{-0.06}) \text{ GeV}, \\ M_Z &= (91.19 \pm 0.002) \text{ GeV}, \quad M_W = (80.42 \pm 0.003) \text{ GeV}, \\ \alpha(M_Z^2) &= 1/127.916 \pm 0.015, \quad \alpha_s(M_Z^2) = 0.1184 \pm 0.0014. \end{aligned} \quad (9)$$

The pMSSM parameters are varied in an uncorrelated way in flat scans, within the following ranges:

$$\begin{aligned} 1 &\leq \tan \beta \leq 60, \\ 50 \text{ GeV} &\leq M_A \leq 3 \text{ TeV}, \\ -10 \text{ TeV} &\leq A_f \leq 10 \text{ TeV}, \\ 50 \text{ GeV} &\leq m_{\tilde{f}_L}, m_{\tilde{f}_R}, M_3 \leq 3.5 \text{ TeV}, \\ 50 \text{ GeV} &\leq M_1, M_2, |\mu| \leq 2.5 \text{ TeV} \end{aligned} \quad (10)$$

to generate a total of 6×10^7 pMSSM points. The scan range is explicitly chosen to include the various mixing scenarios in the Higgs section discussed in section 2.1: the maximal mixing, no-mixing and typical mixing scenarios. Additional 10^7 points are generated in specialised scans used for the studies discussed later in section 3.5. We select the set of points fulfilling constraints from flavour physics and lower energy searches at LEP2 and the Tevatron, as discussed in Ref. [33], to which we refer also for details on the scans. We highlight here the tools most relevant to this study. The SUSY mass spectra are generated with **SuSpect** [16] and **SOFTSUSY** 3.2.3 [17]. The superparticle partial decay widths and branching fractions are computed using the program **SDECAY** 1.3 [34]. The flavour observables and dark matter relic density are calculated with **SuperIso Relic v3.2** [35].

The Higgs production cross sections at the LHC are computed using **HIGLU** 1.2 [36] for the $gg \rightarrow h/H/A$ process, including the exact contributions of the top and bottom quark loops at NLO-QCD and the squark loops, and the program **bb@nnlo** for $b\bar{b} \rightarrow h/H/A$ at NNLO-QCD. They are interfaced with **Suspect** for the MSSM spectrum and **HDECAY** for the Higgs decay branching ratios. The Higgs production cross sections and the branching fractions for decays into $b\bar{b}$, $\gamma\gamma$, WW and ZZ from **HIGLU** and **HDECAY** are compared to those predicted by **FeynHiggs**. In the SM both the $gg \rightarrow H_{SM}$ cross section and the branching fractions agree within $\sim 3\%$. Significant differences are observed in the SUSY case, with **HDECAY** giving values of the branching fractions to $\gamma\gamma$ and WW , ZZ which are on average 9% lower and 19% larger than those of **FeynHiggs** and have an r.m.s. spread of the distribution of the relative difference between the two programs of 18% and 24%, respectively [5].

3.2 Constraints

We apply constraints from flavour physics, anomalous muon magnetic moment, dark matter constraints and SUSY searches at LEP and the Tevatron. These have been discussed in details in Ref. [33]. In particular, we consider the decay $B_s \rightarrow \mu^+ \mu^-$, which can receive extremely large SUSY contributions at large $\tan \beta$. An excess of events in this channels has been reported by the CDF-II collaboration at the Tevatron [37] and upper limits by the LHCb [38] and CMS [39] collaborations at LHC. Recently the LHCb collaboration has presented their latest result for the search of this decay based on 1 fb^{-1} of data. A 95% C.L. upper limit on its branching fraction is set at 4.5×10^{-9} [38]. After accounting for theoretical uncertainties, estimated at the 11% level [40] the constraint

$$\text{BR}(B_s \rightarrow \mu^+ \mu^-) < 5 \times 10^{-9} \quad (11)$$

is used in this analysis. For large values of $\tan \beta$, this decay can be enhanced by several orders of magnitude so that strong constraints on the scalar contributions can be derived [41], and the small M_A and large $\tan \beta$ region can be severely constrained. As already remarked in Ref. [33], the constraints obtained are similar and complementary to those from the dark matter direct detection limits of XENON-100 [42] and searches for the $A \rightarrow \tau^+ \tau^-$ decay.

Concerning the relic density constraint, we impose the upper limit derived from the WMAP-7 result [43]

$$10^{-4} < \Omega_\chi h^2 < 0.155, \quad (12)$$

accounting for theoretical and cosmological uncertainties [44].

The searches conducted by the ATLAS and CMS collaborations on the $\sqrt{s} = 7 \text{ TeV}$ data for channels with missing E_T [45, 46] have already provided a number of constraints relevant to this study. These have excluded a fraction of the pMSSM phase space corresponding to gluinos below $\sim 600 \text{ GeV}$ and scalar quarks of the first two generations below $\sim 400 \text{ GeV}$. These constraints are included using the same analysis discussed in Ref. [33], extended to an integrated luminosity of 4.6 fb^{-1} .

Then, searches for the MSSM Higgs bosons in the channels $h/H/A \rightarrow \tau^+ \tau^-$ [47, 48] have already excluded a significant fraction of the $[M_A, \tan \beta]$ plane at low M_A values, $M_A \lesssim 200 \text{ GeV}$ and $\tan \beta \lesssim 10$, and larger values of $\tan \beta$ for $M_A \gtrsim 200 \text{ GeV}$. These constraint on the pMSSM parameter space are already important. It is supplemented by the search of light charged Higgs bosons in top decays, $t \rightarrow b H^\pm \rightarrow b \tau \nu$, performed by the ATLAS collaboration [49] which is effective at low M_A values, $M_A \lesssim 140 \text{ GeV}$, corresponding to $M_{H^\pm} \lesssim 160 \text{ GeV}$.

Following the Higgs discovery at the LHC, the lightest Higgs boson in our analysis is restricted to have a mass in the range allowed by the results reported by ATLAS and CMS:

$$123 \text{ GeV} \leq M_h \leq 129 \text{ GeV} \quad (13)$$

where the range is centred around the value corresponding to the average of the Higgs mass values reported by ATLAS and CMS, $M_h \simeq 126 \text{ GeV}$, with the lower and upper limits accounting for the parametric uncertainties from the SM inputs given in eq. (9), in particular the top quark mass, and the theoretical uncertainties in the determination of the h boson mass. It is also consistent with the experimental exclusion bounds.

The impact of the Higgs mass value and its decay rates on the parameters of the pMSSM can be estimated by studying the compatibility of the pMSSM points with the first results reported by ATLAS [1] and CMS [2] at the LHC and also by the Tevatron experiments [3]. Starting from our set of 6×10^7 pMSSM points which are pre-selected for compatibility with the constraints discussed above, we consider the two decay channels giving the Higgs boson evidence at the LHC, $\gamma\gamma$ and ZZ and include also the $b\bar{b}$ and $\tau\tau$ channels. In the following, we use the notation R_{XX} to indicate the Higgs decay branching fraction to the final state XX , $\text{BR}(h \rightarrow XX)$, normalised to its SM value. We also compute the ratios of the product of production cross sections times branching ratios for the pMSSM points to the SM values, denoted by μ_{XX} for a given $h \rightarrow XX$ final state, $\mu_{XX} = \frac{\sigma(h) \times \text{BR}(h \rightarrow XX)}{\sigma(H_{\text{SM}}) \times \text{BR}(H_{\text{SM}} \rightarrow XX)}$. These are compared to the experimental values. For the $\gamma\gamma$, and ZZ channels we take a weighted average of the results just reported by the experiments, as given in Table 1 with their estimated uncertainties.

Parameter	Value	Experiment
M_H	125.9 ± 2.1 GeV	ATLAS [1] + CMS [2]
$\mu_{\gamma\gamma}$	1.71 ± 0.33	ATLAS [50] + CMS [51]
μ_{ZZ}	0.95 ± 0.40	ATLAS [52] + CMS [53]
$\mu_{b\bar{b}}$	< 1.64 (95% C.L.)	CMS [54]
$\mu_{\tau\tau}$	< 1.06 (95% C.L.)	CMS [55]

Table 1: Input parameters used for the pMSSM study.

While the results are compatible with the SM expectations within the present accuracy, they highlight a possible enhancement in the observed rates for the $\gamma\gamma$ channel, where ATLAS and CMS obtain $\mu_{\gamma\gamma} = 1.9 \pm 0.5$ and 1.56 ± 0.43 , respectively. In the following, we do not take into account the theoretical uncertainties in the production cross section, which are estimated significant for the main production channel, $gg \rightarrow h$ [56, 57].

3.3 The decoupling regime

Figure 2 presents the parameter space $[M_A, \tan\beta]$ in our benchmark scenario with $M_S = 2$ TeV in the maximal mixing scenario. The regions excluded by the various constraints that we have imposed are indicated. The green area corresponds to the non-observation of Higgs bosons at LEP2 which excludes $\tan\beta \lesssim 3$ at moderate to large M_A values, $M_A \gtrsim 150$ GeV, but up to $\tan\beta \approx 5$ –10 at low M_A values. The blue area is the one ruled out by the latest published results of the CMS collaboration on the search of resonances decaying into $\tau^+\tau^-$ final states; it touches the LEP2 band at small M_A , but reduces in size when M_A is increased. The small visible area in red is the one excluded by the $B_s \rightarrow \mu^+\mu^-$ constraint but, in fact, part of the excluded region is hidden by the CMS blue area.

To that, we superimpose the area in which we make the requirement $123 \leq M_H \leq 129$ GeV, that is indicated in dark blue. This band covers the entire range of M_A values and leaves only the $\tan\beta$ values that are comprised between $\tan\beta \approx 3$ –5 and $\tan\beta \approx 10$. Between the LEP2 and the “ M_h ” blue band, one has $M_h < 123$ GeV, while above the M_h band, one has $M_h > 129$ GeV and both areas are excluded. The requirement that the h boson mass should

have the value measured at the LHC, even with the large uncertainty that we assume, provides thus a strong constraint on the $[M_A, \tan \beta]$ parameter space in the pMSSM.

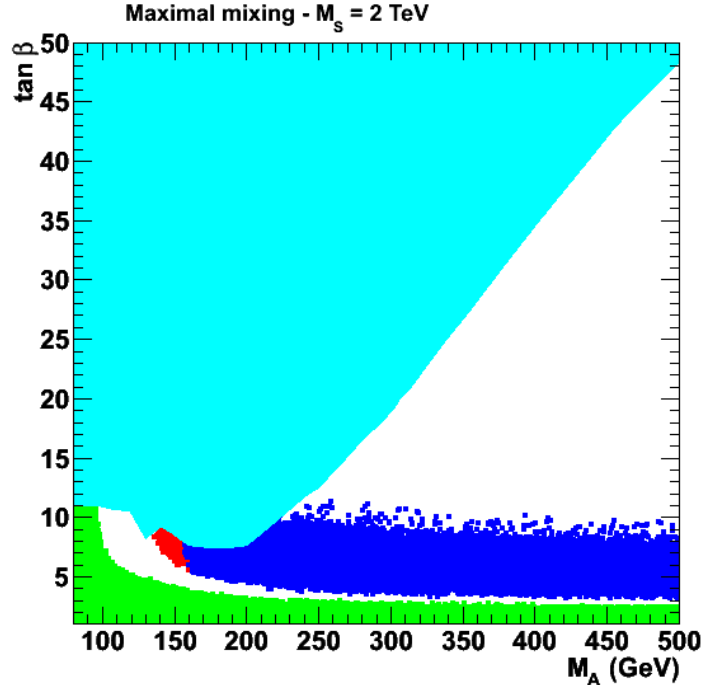


Figure 2: The parameter space $[M_A, \tan \beta]$ for $M_S = 2$ TeV in the maximal mixing scenario with the individual constraints from LEP2 (green), CMS $\tau^+\tau^-$ searches (light blue) and flavor physics (red) displayed. The area in which $123 \leq M_H \leq 129$ GeV is also shown (dark blue).

In Figure 3, we show the same $[M_A, \tan \beta]$ plane but for different SUSY-breaking scales, $M_S = 1, 2$ and 3 TeV and for the zero, typical and maximal mixing scenarios defined in eqs. (4–6). As can be seen, the situation changes dramatically depending on the chosen scenario. Still, in the maximal mixing scenario with $M_S = 3$ TeV the size of the M_h band is reduced from above, as in this case, already values $\tan \beta \gtrsim 5$ leads to a too heavy h boson, $M_h \gtrsim 129$ GeV. In turn, for $M_S = 1$ TeV, the entire space left by the LEP2 and CMS Higgs constraints is covered with many points at $\tan \beta \gtrsim 20$ excluded by the flavor constraint. Nevertheless, the possibility with $M_S \approx 1$ TeV will start to be challenged by the search for squarks at the LHC when 30 fb^{-1} of data will be collected by the experiments. In the no-mixing scenario, it is extremely hard to obtain a Higgs mass of $M_h \geq 123$ GeV and all parameters need to be maximised: $M_S = 3$ TeV and $\tan \beta \gtrsim 20$; a small triangle is thus left over, the top of which is challenged by the flavor constraints. The typical mixing scenario resembles to the no-mixing scenario, with the notable difference that for $M_S = 3$ TeV, the entire space not excluded by the LEP2 and CMS constraints allow for an acceptable value of M_h .

In the discussion so far, we have adopted the value $m_t = (173 \pm 1)$ GeV for the top quark mass as measured by the CDF and D0 experiments at the Tevatron [58]. This implicitly assumes that this mass corresponds to the top quark pole mass, i.e. the mass in the on-shell scheme, which serves as input in the calculation of the radiative corrections in the pMSSM Higgs sector and, in particular, to the mass M_h . However, the mass measured at the Tevatron

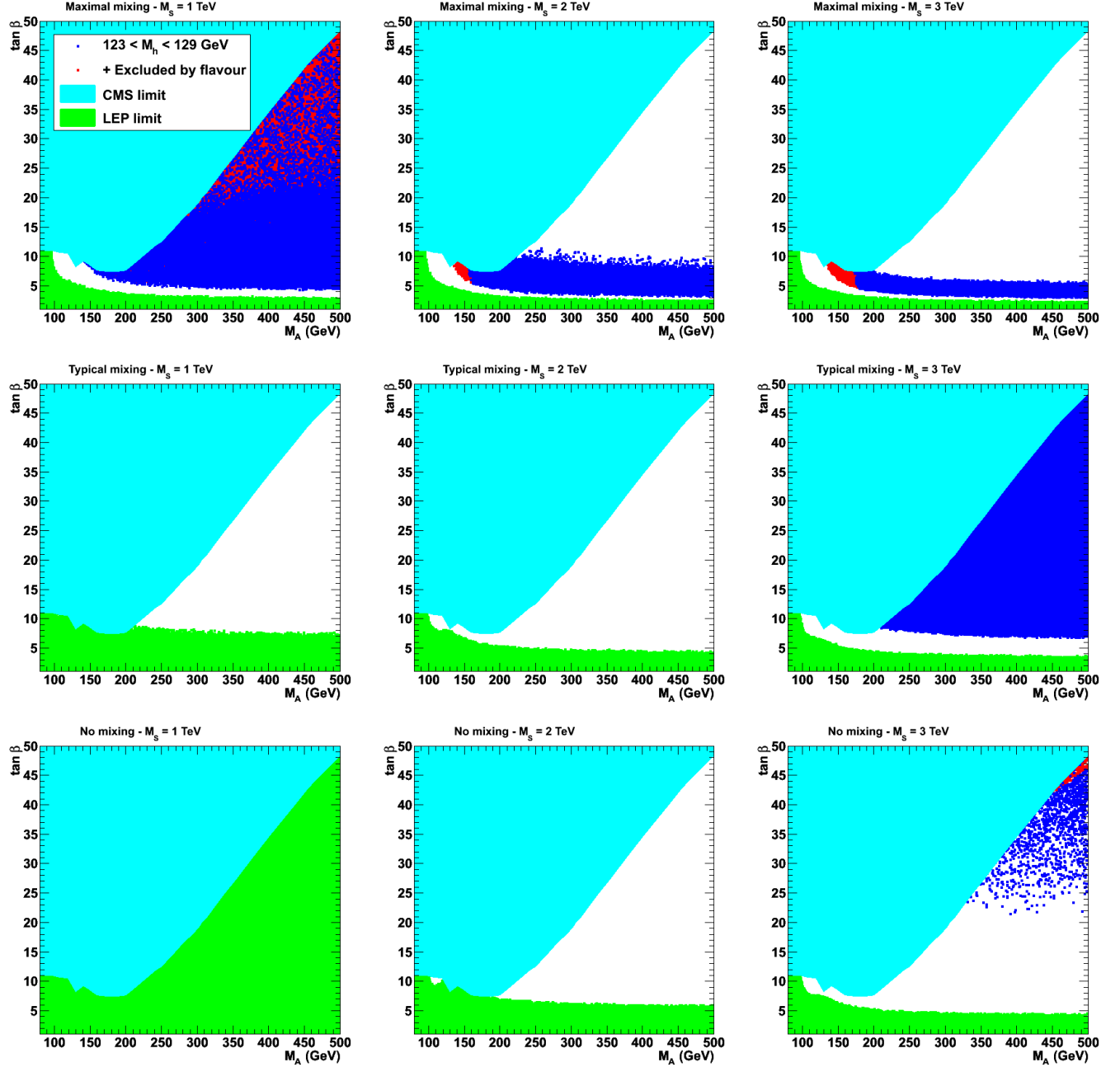


Figure 3: The $[M_A, \tan \beta]$ plane for $M_S = 1, 2$ and 3 TeV and for zero, typical and maximal mixing. The colour coding for the different regions is the same as in Fig. 2.

is not theoretically well defined and it is not proved that it corresponds indeed to the pole mass as discussed in [59]. For an unambiguous and well-defined determination of the top quark mass, it appears to be safer to use the value obtained from the determination of the top quark pair production cross section measured at the Tevatron, by comparing the measured value with the theoretical prediction at higher orders. This determination has been recently performed yielding the value of (173.3 ± 2.8) GeV [59] for m_t^{pole} . The central value is very close to that

measured from the event kinematics but its uncertainty is larger as a result of the experimental and theoretical uncertainties that affect the measurement.

It is interesting to assess the impact of a broader mass range for the top quark. We return to our benchmark scenario with $M_S = 2$ TeV and maximal stop mixing and draw the “ M_h ” bands using the top quark mass values of 170 GeV and 176 GeV corresponding to the wider uncertainty interval quoted above. The result is shown in Figure 4. A 1 GeV change in m_t input leads to a ~ 1 GeV change in the corresponding M_h value. The smaller value of m_t would open up more parameter space as the region in which $M_h \gtrsim 129$ GeV will be significantly reduced. In turn, for $m_t = 176$ GeV, the corresponding h boson mass increases and the dark-blue area quite significantly shrinks, as a result. It must be noted that for $m_t = 170$ GeV, the no-mixing scenario would be totally excluded for $M_S \lesssim 3$ TeV, while in the typical mixing scenario only a small area at high $\tan\beta$ will remain viable. For $m_t = 176$ GeV significant $[M_A, \tan\beta]$ regions that was excluded when taking the ± 1 GeV uncertainty for top mass value becomes allowed. The impact of the value of m_t is thus extremely significant. This is

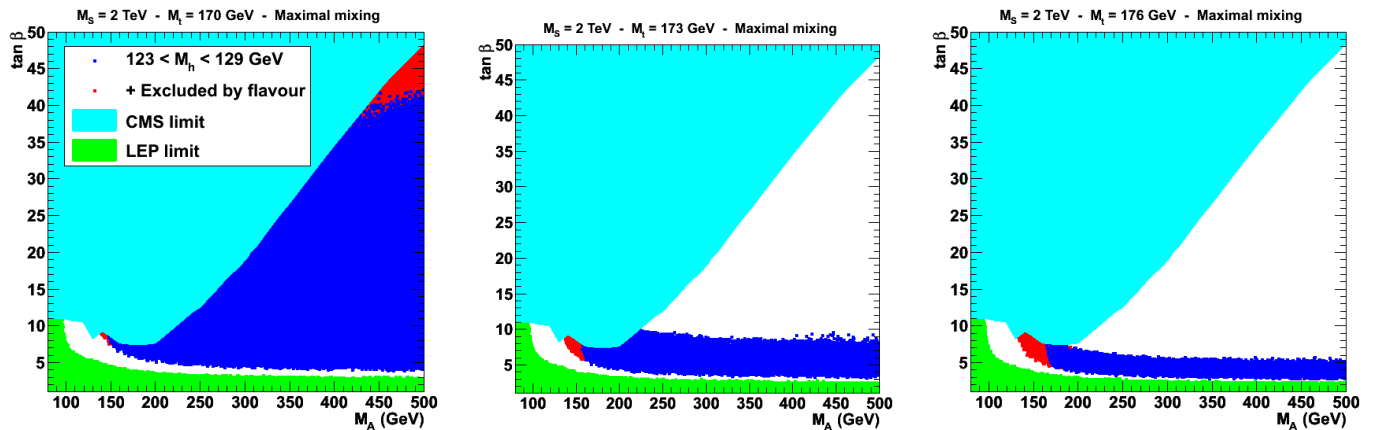


Figure 4: The parameter space $[M_A, \tan\beta]$ for $M_S = 2$ TeV, maximal mixing and three values of the top quark mass $m_t = 170$ GeV (left), 173 GeV (centre) and 176 GeV (right).

even more true in constrained scenarios, where the top mass also enters in the evaluation of the soft SUSY-breaking parameters and the minimisation of the scalar potential. To visualise the impact of m_t , we have repeated the study presented in Ref. [4], presenting the maximal M_h value reached when scanning over all the parameters of the minimal SUGRA, AMSB and GMSB models. Figure 5 shows the result with the M_h^{\max} value as a function of M_S taking $m_t = 173 \pm 3$ GeV. While for $m_t = 173$ GeV, there is no region of the parameter space of the mAMSB and mGMSB models which satisfies $M_h \gtrsim 123$ GeV, for $M_S \lesssim 3$ TeV assumed in [4], and the models are disfavoured, using $m_t = 176$ GeV, the regions of these mAMSB and mGMSB models beyond $M_S = 2$ TeV become again viable. This will be also the case of some of the variants and even more constrained mSUGRA scenarios. Further, even for $m_t = 173$ GeV, if we move the M_S upper limit from the 3 TeV boundary adopted in Ref. [4] to $M_S = 5$ TeV, these models have region of their parameters compatible with the LHC Higgs mass.

Finally, we comment on the impact of increasing the M_h allowed range from $123 \text{ GeV} \leq M_h \leq 127 \text{ GeV}$ as was done in Ref. [4] relying on the 2011 LHC data, to the one adopted here, $123 \text{ GeV} \leq M_h \leq 129 \text{ GeV}$, in the various constrained models discussed in that reference (and to which we refer for the definition of the models and for the ranges of input parameters that

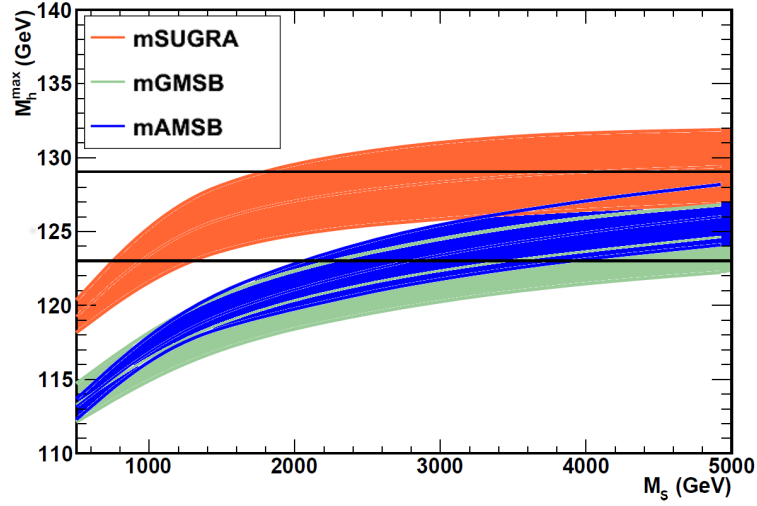


Figure 5: Maximal Higgs mass in the constrained MSSM scenarios mSUGRA, mAMSB and mGMSB, as a function of the scale M_S when the top quark mass is varied in the range $m_t = 170\text{--}176$ GeV.

have been adopted). The outcome is shown in Fig. 6 where the maximal h mass value obtained by scanning the basic input parameters of the model over the appropriate ranges. In the left-hand side, M_h^{\max} is displayed as a function of $\tan\beta$ and in the right-hand side as a function of M_S . As the lower bound $M_h^{\max} \geq 123$ GeV is the same as in our previous analysis, the mAMSB, mGMSB and some variants of the mSUGRA model such as the constrained NMSSM (cNMSSM), the no-scale model and the very constrained MSSM (VCMSSM) scenarios are still disfavoured. However, for mSUGRA and the non-universal Higgs mass model (NUHM), all values of $\tan\beta \gtrsim 3$ and $1\text{ TeV} \lesssim M_S \lesssim 3\text{ TeV}$ lead to an appropriate value of M_h when including the uncertainty band.

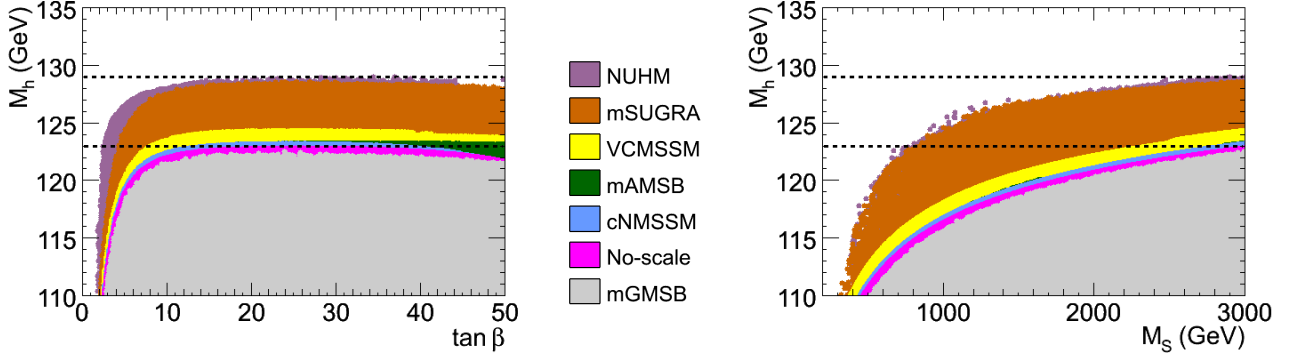


Figure 6: The maximal h mass value M_h^{\max} as functions of $\tan\beta$ (left) and M_S (right) in the mAMSB, mGMSB as well as in mSUGRA and some of its variants. The basic parameters of the models are varied within the ranges given in Ref. [4]; the top quark mass is fixed to $m_t = 173$ GeV.

3.4 The other (non-SUSY) regimes

The other regimes of the pMSSM Higgs sector, apart from the decoupling and the SUSY regimes, occur for low to intermediate values of the pseudoscalar Higgs mass, $M_A \lesssim 200$ GeV, and relatively large $\tan \beta$ values. These are the anti-decoupling, the intense, the intermediate and the vanishing coupling regimes. These are constrained by the results of the LEP2 and LHC searches. The LEP2 results for $M_A \lesssim 200$ GeV and not too large M_S values, lead to $\tan \beta \gtrsim 3, 8$ and 10 for, respectively the maximal, typical and no-mixing scenarios; see Fig. 3. The negative search for Higgs particles in τ -lepton final states, $pp \rightarrow \Phi \rightarrow \tau^+\tau^-$, by the ATLAS and CMS collaborations places further constraints. While in the decoupling regime, the relevant Higgs states would be $\Phi = A + H$, these are $\Phi = A + h$ and $\Phi = A + H + h$ in the anti-decoupling and intense coupling regimes, respectively. As already mentioned, one would have in the three regimes the same signal cross section times branching ratios $\sigma(pp \rightarrow \Phi \rightarrow \tau^+\tau^-) \approx \sigma(b\bar{b} + gg \rightarrow A) \times \text{BR}(A \rightarrow \tau^+\tau^-)$ almost independently of the mixing scenario and the other pMSSM parameters [57]. The constraint from the CMS published results alone with the $\approx 5 \text{ fb}^{-1}$ of data collected in 2011 [48] imposes $\tan \beta \gtrsim 10$, as shown in Fig. 7 where we zoom on the plane $[M_A, \tan \beta]$ at low to intermediate M_A values, for the maximal mixing scenario and $M_S = 2$ TeV.

This limit can be strengthened by the same $\tau^+\tau^-$ search performed by the ATLAS collaboration [47] and also by the $t \rightarrow H^+b$ search in top decays [49] which is effective for $M_A = \sqrt{M_{H^\pm}^2 + M_W^2} \lesssim 130$ GeV and which, as can be seen in Fig. 7, excludes large $\tan \beta$ values for which $\text{BR}(t \rightarrow bH^+)$ is significant. Put together, these constraints exclude entirely both the anti-decoupling and intense coupling regimes. Would remain then, the intermediate coupling regime with $\tan \beta \approx 5$ – 8 when the LEP2 constraint is also imposed. Depending on the mixing scenario, most of it will be excluded by the $M_h \approx 126$ GeV constraint (see Fig. 3).

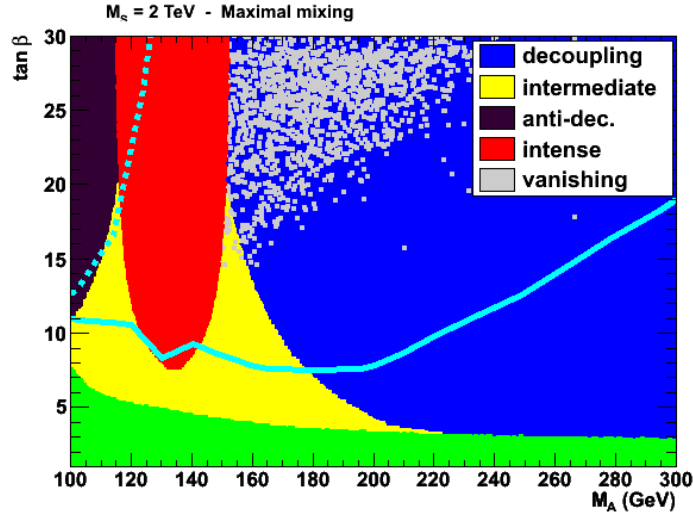


Figure 7: Parameter space for the various regimes of the MSSM Higgs sector as defined in the text and in eq. (8) in the $[M_A, \tan \beta]$ plane, in the maximal mixing scenario with $M_S = 2$ TeV. The upper limit constraints from $\Phi \rightarrow \tau\tau$ (continuous light blue line) and $t \rightarrow H^+b$ (dashed blue line) searches at the LHC are shown together with the LEP2 excluded region (green area).

A very interesting possibility would be that the observed Higgs particle at the LHC is

actually the H state, while the lighter h boson has suppressed couplings to W/Z bosons and top quarks, allowing it to escape detection. In this case, the H couplings to bottom quarks should not be too enhanced, $\tan\beta \lesssim 8$, not to be in conflict with the $\tau^+\tau^-$ and $t \rightarrow bH^+$ searches above. For the H boson to be SM-like, one should have $M_A \approx M_H \approx 126$ GeV and not too low $\tan\beta$ values, $\tan\beta \gtrsim 7$ –10. One is then in the borderline between the anti-decoupling and the intermediate coupling regimes. We have searched for points in which indeed $M_H \approx 126$ GeV with couplings to VV states, $g_{HVV} \gtrsim 0.9$, such that the $H \rightarrow ZZ$ and $H \rightarrow \gamma\gamma$ (which mainly occurs through a W -boson loop) decays are not suppressed compared to the measured values by ATLAS and CMS given in Table 1. In our scan, out of the 10^6 points, before imposing any LHC–Higgs constraint, only ≈ 20 points fulfilled the above requirements. These points are then completely excluded once the flavor constraints, in particular those from the $b \rightarrow s\gamma$ radiative decay, are imposed. Hence, the possibility that the observed Higgs particle at the LHC is not the lightest h particle appears highly unlikely according to the result of our scan of the parameter space. Combining the $h/A \rightarrow \tau^+\tau^-$ and the $t \rightarrow bH^+$ constraints and including the results on the new 8 TeV data should further constrain the parameter space and completely exclude this scenario.

Finally, the vanishing coupling regime is strongly disfavoured by the LHC and Tevatron data that are summarised in Table 1. The observation of $H \rightarrow ZZ$ final states by the ATLAS and CMS collaborations rules out the possibility of vanishing hVV couplings. The reported excess of events in the $q\bar{q} \rightarrow VH \rightarrow Vb\bar{b}$ process by the CDF and D0 collaborations seem also to rule out both the vanishing hbb and hVV coupling scenarios. However, there is still the possibility that these couplings are smaller than those predicted in the SM case, in particular because of the effects of SUSY particles at high $\tan\beta$ [24]. We are then in the SUSY-regime to which we turn now.

3.5 The SUSY regime

In the SUSY regime, both the Higgs production cross section in gluon–gluon fusion and the Higgs decay rates can be affected by the contributions of SUSY particles. This makes a detailed study of the pMSSM parameter space in relation to the first results reported by the ATLAS and CMS collaborations especially interesting for its sensitivity to specific regions of the pMSSM parameter space. In particular, the branching fraction for the $\gamma\gamma$ decay of the h state is modified by Higgs mixing effects outside the decoupling regime as was discussed above, by a change of the hbb coupling due to SUSY loops [24], by light superparticle contributions to the $h\gamma\gamma$ vertex [6, 25, 26] and by invisible h decays into light neutralinos [28].

We study these effects on the points of our pMSSM scan imposing the LHC results as constraints. The numerical values adopted in the analysis are given in Table 1, assuming in the following on that the observed particle is the h state. First, we briefly summarise the impact of the SUSY particles on the Higgs decay branching fractions, starting from invisible decays, and production cross sections. Then we discuss our finding on the impact of the LHC and Tevatron data on the pMSSM parameters.

3.5.1 Invisible Higgs decays

Despite the fact that the discovered particle has a sufficient event rate in visible channels to achieve its observation, it is interesting to consider the regions of parameter space in which invisible Higgs decays occur. This scenario has recently been re-considered in [5, 30]. Besides the value of M_h , the invisible branching ratio $\text{BR}(h \rightarrow \chi_1^0 \chi_1^0)$ is controlled by four parameters: the gaugino masses M_1 and M_2 , the higgsino parameter μ and $\tan \beta$. They enter the 4×4 matrix Z which diagonalises the neutralino mass matrix. They also enter the Higgs coupling to neutralinos which, in the case of the LSP, is

$$g_{h\chi_1^0\chi_1^0} \propto (Z_{12} - \tan \theta_W Z_{11}) (\sin \beta Z_{13} + \cos \beta Z_{14}) \quad (14)$$

if we assume the decoupling limit not to enhance the $h \rightarrow b\bar{b}$ channel which would significantly reduce the invisible decay. In this coupling, Z_{11}, Z_{12} are the gaugino components and Z_{13}, Z_{14} the higgsino components. Thus, the coupling vanishes if the LSP is a pure gaugino, $|\mu| \gg M_1$ leading to $m_{\chi_1^0} \approx M_1$, or a pure higgsino, $M_1 \gg |\mu|$ with $m_{\chi_1^0} \approx |\mu|$.

For the invisible decay to occur, a light LSP, $m_{\chi_1^0} \leq \frac{1}{2}M_h$ is required. Since in the pMSSM, the gaugino mass universality $M_2 \approx 2M_1$ is relaxed, one can thus have a light neutralino without being in conflict with data. The constraint from the Z invisible decay width measured at LEP restricts the parameter space to points where the $\tilde{\chi}_1^0$ is bino-like, if its mass is below 45 GeV, and thus to relatively large values of the higgsino mass parameter $|\mu|$. Since a large decay width into $\tilde{\chi}_1^0 \tilde{\chi}_1^0$ corresponds to small values of $|\mu|$, this remove a large part of the parameter space where the invisible Higgs decay width is sizable. Still, we observe invisible decays for $45 \text{ GeV} < M_{\tilde{\chi}_1^0} < M_{h^0}/2$ and $|\mu| < 150$, corresponding to a combination of parameters where the $\tilde{\chi}_1^0$ is a mixed higgsino-gaugino state [5]. These pMSSM points are shown in the $[M_1, \mu]$ plane in the left panel of Fig. 8.

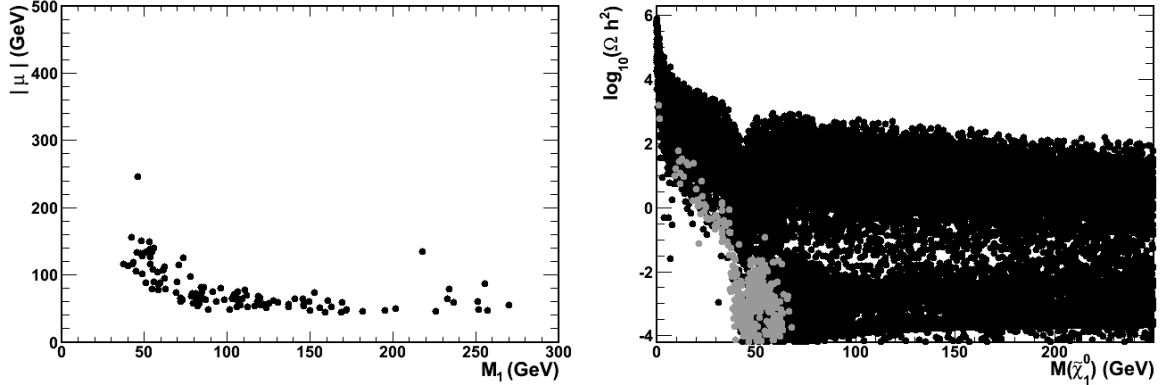


Figure 8: Left: Points in the $[M_1, \mu]$ parameter space where the invisible branching fraction $\text{BR}(h \rightarrow \chi_1^0 \chi_1^0) \geq 0.15$ from a pMSSM scan where we impose the LEP constraint on the Z invisible width and neutralino relic density $\Omega_{\tilde{\chi}_1^0} h^2$. Right: $\Omega_{\tilde{\chi}_1^0} h^2$ as a function of $m_{\chi_1^0}$ with all the selected pMSSM points in black and those giving a $\text{BR}(h \rightarrow \chi_1^0 \chi_1^0) \geq 0.15$ in grey.

If the LSP at such a low mass were to be the dark-matter particle, with the relic density given in eq. (12), it should have an efficient annihilation rate into SM particles. The only possible way for that to occur would be $\chi_1^0 \chi_1^0$ annihilation through the s -channel light h

pole³ [60] which implies that $m_{\chi_1^0} \lesssim \frac{1}{2}M_h$ to still have a non-zero invisible branching ratio, as shown in the right panel of Fig. 8, where the pMSSM points satisfying $\text{BR}(h \rightarrow \chi_1^0 \chi_1^0) \geq 5\%$ are shown in the plane $[m_{\chi_1^0}, \log_{10}(\Omega h^2)]$. However, because the partial decay width $\Gamma(h \rightarrow \chi_1^0 \chi_1^0)$ is suppressed by a factor β^3 near the $M_h \approx 2m_{\chi_1^0}$ threshold, with the velocity $\beta = (1 - 4m_{\chi_1^0}^2/M_h^2)^{1/2}$, the invisible branching fraction is rather small if the WMAP dark matter constraint is to hold. MSSM light neutralinos compatible with claims of direct detection dark matter signals are also consistent with collider bounds [61].

3.5.2 Sparticle effects on the $h b \bar{b}$ coupling

SUSY particles will contribute to the $h b \bar{b}$ coupling as there are additional one-loop vertex corrections that modify the tree-level Lagrangian that incorporates them [24]. These corrections involve bottom squarks and gluinos in the loops, but there are also possibly large corrections from stop and chargino loops. Both can be large since they grow as $\mu \tan \beta$ or $A_t \mu \tan \beta$ [24]

$$\Delta_b \approx \frac{2\alpha_s}{3\pi} \frac{m_{\tilde{g}} \mu \tan \beta}{\max(m_{\tilde{g}}^2, m_{\tilde{b}_1}^2, m_{\tilde{b}_2}^2)} + \frac{m_t^2}{8\pi^2 v^2 \sin^2 \beta} \frac{A_t \mu \tan \beta}{\max(\mu^2, m_{\tilde{t}_1}^2, m_{\tilde{t}_2}^2)}. \quad (15)$$

Outside the decoupling limit, the reduced $b \bar{b}$ couplings of the h state are given in this case by

$$g_{hbb} \approx g_{Abb} \approx \tan \beta (1 - \Delta_b) \quad (16)$$

and can be thus significantly reduced or enhanced⁴ depending on the sign of μ and, possibly, also A_t . This is exemplified in the left panel of Fig. 9, where the ratio $R_{bb} \equiv \text{BR}(h \rightarrow b \bar{b})/\text{BR}(H_{\text{SM}} \rightarrow b \bar{b})$ is shown as a function of the parameter $\mu \tan \beta$ before the constraints of Table 1. The two branches in the histogram are due to the sbottom and stop contributions in which R_{bb} is increased or decreased depending on the sign of μ .

A deviation of the partial $h \rightarrow b \bar{b}$ width will enter the total Higgs width, which is dominated by the $b \bar{b}$ channel, and change the R values for the different Higgs decay channels. A reduction of R_{bb} would thus lead to an enhancement of the $\gamma\gamma$ and the WW/ZZ branching fractions. Figure 10 shows the values of R_{bb} and $R_{\gamma\gamma}$ in which we observe a highly anti-correlated variation of the two ratios, with the exception of the cases where the opening of the decay $h \rightarrow \chi\chi$ suppresses both branching fractions. The preliminary results from LHC and the Tevatron are overlayed.

3.5.3 Sparticle contributions to the $h g g$ and $h \gamma \gamma$ vertices

Scalar top quarks can alter significantly the $g g \rightarrow h$ cross section as well as the $h \rightarrow \gamma\gamma$ decay width [25]. The current eigenstates \tilde{t}_L, \tilde{t}_R mix strongly, with a mixing angle $\propto m_t X_t$, so that

³The other possible channels are strongly suppressed or ruled out. The co-annihilation with charginos, heavier neutralinos and staus is not effective as these particles need to be heavier than ≈ 100 GeV and thus the mass difference with the LSP is too large. The annihilation through the A -pole needs $M_A \approx 2m_{\chi_1^0} \lesssim M_h$ and sizable $\tan \beta$ values, which is the anti-decoupling regime that is excluded as discussed above. Remains then the bulk region with staus exchanged in the t -channel in $\chi_1^0 \chi_1^0 \rightarrow \tau^+ \tau^-$ (sbottoms are too heavy) which is difficult to enhance as the LSP is bino-like.

⁴These corrections also affect the Higgs production cross sections in the channels $g g + b \bar{b} \rightarrow \Phi$. However, in the cross sections times branching ratios for the $\tau^+ \tau^-$ final states, they almost entirely cancel as they appear in both the production rate and the total Higgs decay width [57].

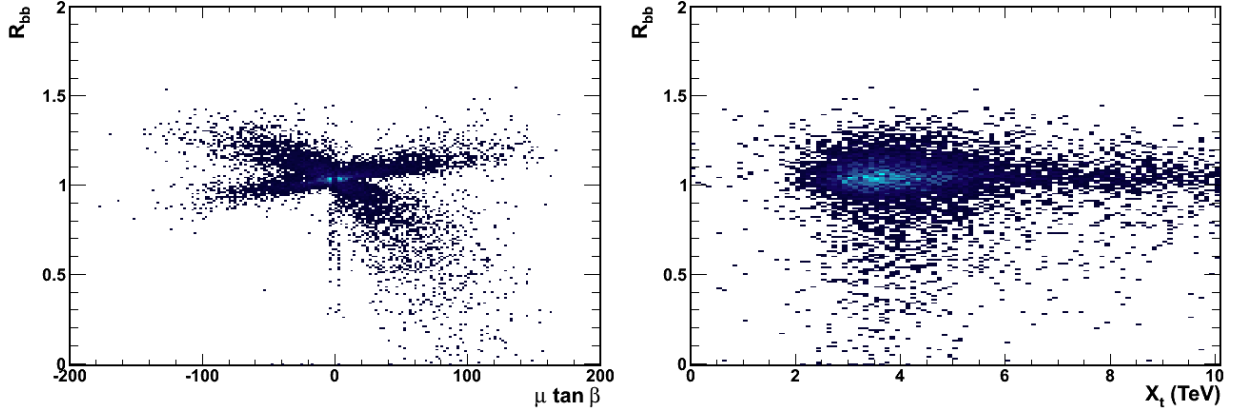


Figure 9: (Left) R_{bb} values for a sample of pMSSM points as a function of the product of the $\mu \tan \beta$ showing the reduction at large values of $\mu \tan \beta$. The reduction in a narrow strip at small values of μ is due to decays into $\chi\chi$. (Right) the same as a function of A_t .

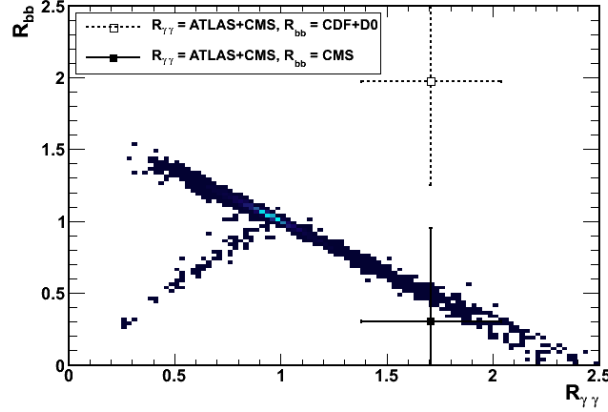


Figure 10: R_{bb} as a function of $R_{\gamma\gamma}$, showing their anti-correlated variation; the points corresponding to a decrease of both ratios are due to an enhancement of invisible decays to light neutralinos. The values of $R_{\gamma\gamma}$ obtained by ATLAS+CMS and R_{bb} corresponding to the CMS and CDF+D0 searches are overlaid as comparison.

for large $X_t = A_t - \mu/\tan \beta$ values⁵ there is a lighter mass eigenstate \tilde{t}_1 which can be much lighter than all other scalar quarks, $m_{\tilde{t}_1} \ll M_S$. The coupling of the h boson to the \tilde{t}_1 states in the decoupling regime reads

$$g_{h\tilde{t}_1\tilde{t}_1} = \cos 2\beta M_Z^2 \left[\frac{1}{2} \cos^2 \theta_t - \frac{2}{3} s_W^2 \cos 2\theta_t \right] + m_t^2 + \frac{1}{2} \sin 2\theta_t m_t X_t, \quad \sin 2\theta_t = \frac{2m_t X_t}{m_{\tilde{t}_1}^2 - m_{\tilde{t}_2}^2} \quad (17)$$

In the no-mixing scenario $X_t \approx 0$, the coupling above is $\propto m_t^2$ and the scalar top contribution to the hgg amplitude is small, being damped by a factor $1/m_{\tilde{t}_1}^2$ and interferes constructively with the top quark contribution to increase the $gg \rightarrow h$ rate. However, since in the no-mixing

⁵On should assume X_t values such that $A_t \lesssim 3M_S$ to avoid dangerous charge and colour breaking minima. In addition, if $X_t \gtrsim \sqrt{6}M_S$, the radiative corrections to the h boson mass become small again and it would be difficult to attain the value $M_h \approx 126$ GeV.

scenario $M_S = \sqrt{m_{\tilde{t}_1} m_{\tilde{t}_2}}$ has to be very large for the h boson mass to reach a value $M_h \approx 126$ GeV, the stop contribution to the hgg vertex, $\propto m_t^2/M_S^2$, is very small. In the maximal mixing scenario, $X_t \approx \sqrt{6}M_S$, it is the last component of $g_{h\tilde{t}_1\tilde{t}_1}$ which dominates and becomes very large, $\propto -(m_t X_t/m_{\tilde{t}_2})^2$. However, in this case, the large contribution of a light stop to the hgg amplitude interferes destructively with the top quark contribution and the $gg \rightarrow h$ cross section is suppressed. For $m_{\tilde{t}_1} \approx 200$ GeV and $X_t \approx 1$ TeV, we obtain a factor of two smaller $gg \rightarrow h$ rate. In the case of sbottom squarks, the same situation may occur for large sbottom mixing $X_b = A_b - \mu \tan \beta$. However, for large value of M_S , it is more difficult to obtain a small enough $m_{\tilde{b}_1}$ state to significantly affect the $gg \rightarrow h$ cross section.

In the case of the $h\gamma\gamma$ decay amplitude, there is the additional SM contribution of the W boson, which is in fact the dominant. Also, it has the opposite sign to that from the top quark and, hence, when stops are light and have a strong mixing, they will tend to increase the $h\gamma\gamma$ amplitude. However, because the W contribution is by far the largest, the stop impact will be much more limited compared to the ggh case and we can expect to have only a $\approx 10\%$ increase of the $h \rightarrow \gamma\gamma$ decay rate for $m_{\tilde{t}_1} \approx 200$ GeV and $X_t \approx 1$ TeV [25–27]. Therefore, for light and strongly mixed stops, the cross section times branching ratio $\mu_{\gamma\gamma}$ is always smaller unity and relatively light stops do not entail an enhancement of the $\gamma\gamma$ yield. The sbottom contribution

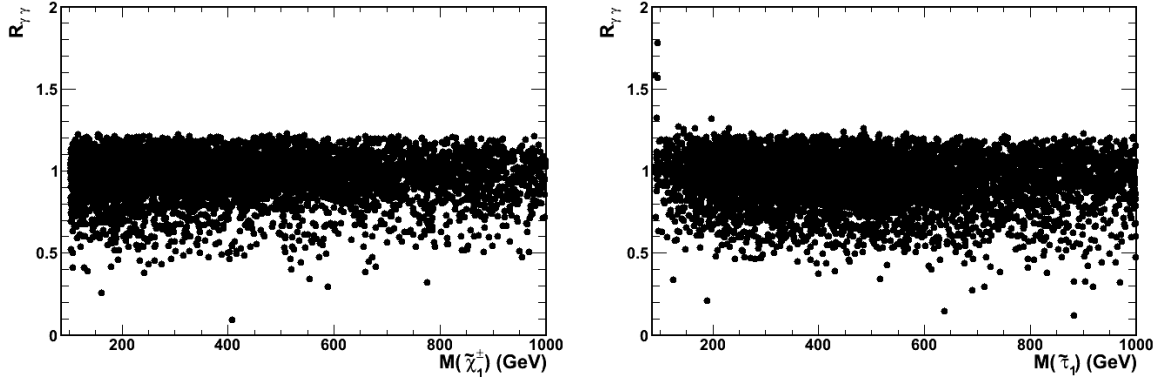


Figure 11: $R_{\gamma\gamma}$ values for a sample of pMSSM points as a function of $m_{\chi_1^\pm}$ (left) and $(m_{\tau_1^\pm})$ (right). We impose $R_{bb} > 0.9$, to remove the effects due to the changes of the total width through the bb channel.

to the $h\gamma\gamma$ vertex is also very small, for the same reasons discussed above in the case of the hgg amplitude, and also because of its electric charge, $-\frac{1}{3}$ compared to $+\frac{2}{3}$ for stops. Other charged particles can also contribute to the $h \rightarrow \gamma\gamma$ rate [26]. The charged Higgs bosons have negligible contributions for $m_{H^\pm} \gtrsim 200$ GeV. Charginos contribute to the $h\gamma\gamma$ vertex and, because of their spin $\frac{1}{2}$ nature, their contribution is only damped by powers of M_h/m_{χ^\pm} . However, the $h\chi_{1,2}^\pm\chi_{1,2}^\mp$ couplings are similar in nature to those of the LSP given in eq. (14) and cannot be strongly enhanced. As a result we expect contributions at most of the order of 10% even for mass values $m_{\chi_1^\pm} \approx 100$ GeV (see Fig. 11). Charged sleptons have in general also little effect on the $h\gamma\gamma$ vertex, with the exception of staus [6]. These behave like the bottom squarks. At very large $\mu \tan \beta$ values, the splitting between the two $\tilde{\tau}$ states becomes significant and their couplings to the h boson large. Since $\tilde{\tau}_1$ can have a mass of the order of a few 100 GeV, without affecting the value of M_h , its contribution to the $h\gamma\gamma$ amplitude may be significant for large values of X_τ (see Fig. 11).

3.5.4 Impact of the LHC data

Now, it is interesting to perform a first assessment of the compatibility of the LHC and Tevatron data with the MSSM and analyse the region of parameter favoured by the observed boson mass and rate pattern (see also [5, 62]). Despite the preliminary character of the results reported by the LHC collaborations and the limited statistical accuracy of these first results, the study is a template for future analyses. In this analysis, we computing the χ^2 probability on the observable of Table 1 for each accepted pMSSM points. For the $b\bar{b}$ and $\tau^+\tau^-$ channels, in which no evidence has been obtained at the LHC, we add the channel contribution to the total χ^2 only when their respective μ value exceeded 1.5 and the pMSSM point becomes increasingly less consistent to the limits reported by CMS. In order to investigate the sensitivity to the inputs, we also compare the results by including or not the $b\bar{b}$, for which a tension exists between the CMS limit and Tevatron results, and the $\tau^+\tau^-$ rate. Figure 12 shows the region of the $[X_t, m_{\tilde{t}_1}]$, $[X_b, m_{\tilde{b}_1}]$ and $[M_A, \tan \beta]$ parameter space where pMSSM points are compatible with the input h boson mass and observed yields. In particular, we observe an almost complete suppression for low values of the sbottom mixing parameter X_b .

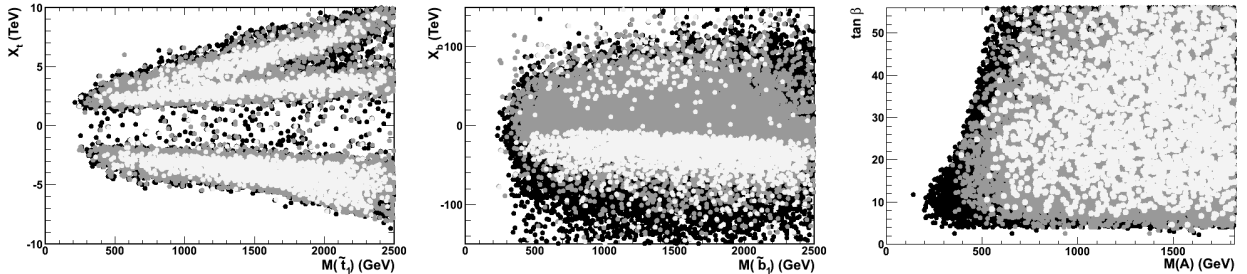


Figure 12: Distributions of the pMSSM points in the $[X_t, m_{\tilde{t}_1}]$ (left), $[X_b, m_{\tilde{b}_1}]$ (centre) and $[M_A, \tan \beta]$ (right) parameter space. The black dots show the selected pMSSM points, those in light (dark) grey the same points compatible at 68% (90%) C.L. with the the Higgs constraints of Table 1.

The distributions for some individual parameters which manifest a sensitivity are presented in Figure 13, where each pMSSM point enters with a weight equal to its χ^2 probability. Points having a probability below 0.15 are not included. The probability weighted distributions obtained from this analysis are compared to the normalised frequency distribution for the same observables obtained for accepted points within the allowed mass region $122.5 < M_H < 127.5$ GeV. We observe that some variables are significantly affected by the constraints applied. Not surprisingly, the observable which exhibits the largest effect is the product $\mu \tan \beta$, for which the data favours large positive values, where the $\gamma\gamma$ branching fraction increases and the $b\bar{b}$ decreases as discussed above. On the contrary, it appears difficult to reconcile an enhancement of both $\mu_{\gamma\gamma}$ and $\mu_{b\bar{b}}$, as would be suggested by the central large value of $\mu_{b\bar{b}} = 1.97 \pm 0.72$ recently reported by the Tevatron experiments [3]. Such an enhancement is not observed by the CMS collaboration and the issue is awaiting the first significant evidence of a boson signal in the $b\bar{b}$ final state at the LHC and the subsequent rate determination. The $\tan \beta$ distribution is also shifted towards larger value as an effect of the Higgs mass and rate values. We also observe a significant suppression of pMSSM points with the pseudo-scalar A boson mass below ~ 450 GeV. This is due to the combined effect of the $A \rightarrow \tau^+\tau^-$ direct searches and $B_s \rightarrow \mu^+\mu^-$ rate, which constrain the $[M_A - \tan \beta]$ plane to low $\tan \beta$ value for light A

masses, by the shift to $\mu \tan \beta$ from the Higgs rates disfavouring the low $\tan \beta$ region and by the suppression of the non-decoupling regime.

In quantitative terms, we observe that 0.06 (0.50) of the selected pMSSM points are compatible with the constraints given in Table 1 at the 68% (90%) confidence level. If we remove the constraint on the upper limit constraint on the $b\bar{b}$ and $\tau^+\tau^-$ rates, the fraction of points accepted at the 90% C.L. does not change significantly, at 0.56, but that at the 68% C.L. doubles to 0.12. On the contrary, if we replace the CMS upper limit for μ_{bb} with the μ_{bb} result of the Tevatron experiments for $M_H = 125$ GeV [3], the fraction of accepted points at 68% C.L. drops below 0.005. This highlights the tension which will be created in the pMSSM by a simultaneous excess in the $\gamma\gamma$ and $b\bar{b}$ channels, excess which cannot be adequately described in the pMSSM, as discussed above (see Figure 10).

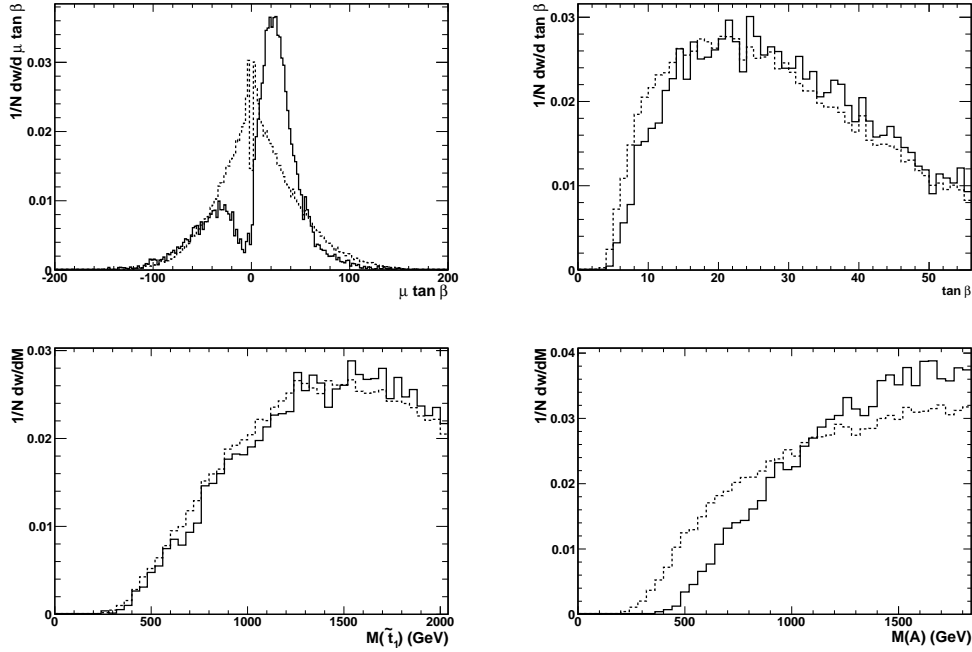


Figure 13: The normalised distribution of the values of the $\mu \tan \beta$ (upper left), $\tan \beta$ (upper right), $M_{\tilde{t}_1}$ (lower left) and M_A (lower right) variables for the selected pMSSM points (dashed line) compared to the probability density function for the same variables obtained from the χ^2 probability using M_h , $R_{\gamma\gamma}$ and R_{ZZ} (continuous line). The normalised distributions reflect the biases induced by the Higgs constraints.

4 Conclusions

The implications of the new boson observation by the ATLAS and CMS collaborations for the phenomenological MSSM have been outlined. The study has been based on broad scans over the pMSSM parameter space where points have been preselected based on constraints from electro-weak and flavour physics, dark matter and searches at LEP2 and the LHC. Various scenarios for the stop mixing parameter X_t (maximal, typical and zero-mixing) and representative values

of the soft SUSY-breaking scale M_S (1, 2 and 3 TeV) have been confronted with the Higgs mass range compatible with LHC results, accounting for systematic uncertainties. In order to obtain M_h in the mass range $123 \text{ GeV} \leq M_h \leq 129 \text{ GeV}$, large values of M_S and/or X_t are required. In particular, the M_h constraints are sensitive to the value of the top quark mass for which the value extracted from the top quark pair production cross section has a more unambiguous definition but larger uncertainties.

The various regimes of the pMSSM Higgs sector have been examined in the $[M_A, \tan \beta]$ parameter. Of these regimes, only the decoupling regime, where the lighter h boson has almost SM-like properties and the heavier Higgs particles decouple from gauge bosons, and the SUSY regime survives all constraints. The anti-decoupling regime where the H state plays the role of the SM Higgs boson, the intense coupling regime in which there are three light states h, H and A , the vanishing coupling regime in which the h coupling to bottom quarks or gauge bosons are very strongly suppressed, and most of the intermediate coupling regime with relatively low M_A and $\tan \beta$ values, are excluded by the present data. In the SUSY regime light superparticles may affect the production and decay rates of the h boson. Light neutralinos may lead to invisible h boson decays, light stop and sbottom quarks affect the $hb\bar{b}$ couplings and the production cross section in the dominant gluon-gluon fusion mechanism, and light squarks, τ -sleptons and charginos may affect the $h \rightarrow \gamma\gamma$ decay mode.

We have confronted these possibilities with the recent LHC results and find that a significant fraction of pMSSM points in our scan compatible with them, including a possible enhancement of the $\gamma\gamma$ rate. Improved precision in the experimental measurements and sensitivity to the direct searches for the heavier Higgs bosons and supersymmetric particle partners at the LHC will provide the basis for clarifying the relation between the newly discovered scalar sector and physics beyond the Standard Model.

Acknowledgements

A.A. and F.M. acknowledge partial support from the European Union FP7 ITN INVISIBLES (Marie Curie Actions, PITN-GA-2011-289442). A.D. thanks the CERN TH unit for hospitality.

References

- [1] [ATLAS Collaboration], CERN-PH-EP-2012-167 and F. Gianotti, for the ATLAS Collaboration, CERN Seminar, July 4th, 2012.
- [2] [CMS Collaboration], CMS PAS HIG-12-020 and J. Incandela, for the CMS Collaboration, CERN Seminar, July 4th, 2012.
- [3] The CDF and D0 Collaborations, FERMILAB-CONF-12-318-E.
- [4] A. Arbey, M. Battaglia, A. Djouadi, F. Mahmoudi and J. Quevillon, Phys. Lett. B708 (2012) 162.
- [5] A. Arbey, M. Battaglia and F. Mahmoudi, Eur. Phys. J. C72 (2012) 1906.
- [6] M. Carena, S. Gori, N. R. Shah and C. E. M. Wagner, JHEP 1203 (2012) 014.

- [7] H. Baer, V. Barger and A. Mustafayev, Phys. Rev. D85 (2012) 075010; S. Heinemeyer, O. Stal and G. Weiglein, Phys. Lett. B710 (2012) 201; P. Draper, P. Meade, M. Reece and D. Shih, Phys. Rev. D85 (2012) 095007; O. Buchmueller, R. Cavanaugh, A. De Roeck, M. J. Dolan, J. R. Ellis, H. Flacher, S. Heinemeyer and G. Isidori *et al.*, arXiv:1112.3564 [hep-ph]; S. Akula, B. Altunkaynak, D. Feldman, P. Nath and G. Peim, Phys. Rev. D85 (2012) 075001 C. Stenge, G. Bertone, D. G. Cerdeno, M. Fornasa, R. R. de Austri and R. Trotta, JCAP 1203 (2012) 030; C. Beskidt, W. de Boer, D. I. Kazakov and F. Ratnikov, JHEP 1205 (2012) 094; M. Carena, S. Gori, N. R. Shah, C. E. M. Wagner and L. -T. Wang, arXiv:1205.5842 [hep-ph]; M. W. Cahill-Rowley, J. L. Hewett, A. Ismail and T. G. Rizzo, arXiv:1206.5800 [hep-ph];
- [8] A. Djouadi and S. Rosiers–Lees (conv.) et al., Summary Report of the MSSM Working Group for the “GDR–Supersymétrie”, hep-ph/9901246.
- [9] A. Djouadi, Phys. Rept. 459 (2008) 1.
- [10] M. Carena and H. Haber, Prog. Part. Nucl. Phys. 50 (2003) 63; S. Heinemeyer, W. Hollik and G. Weiglein, Phys. Rept. 425 (2006) 265; S. Heinemeyer, Int. J. Mod. Phys A21 (2006) 2659.
- [11] A. Djouadi, Phys. Rept. 457 (2008) 1.
- [12] Y. Okada, M. Yamaguchi and T. Yanagida, Prog. Theor. Phys. 85 (1991) 1; J.R. Ellis, G. Ridolfi and F. Zwirner, Phys. Lett. B257 (1991) 83; H.E. Haber and R. Hempfling, Phys. Rev. Lett. 66 (1991) 1815.
- [13] M. Carena, S. Heinemeyer, C. Wagner and G. Weiglein, Eur. Phys. J. C26 (2003) 601.
- [14] B. Allanach et al., JHEP 0409 (2004) 044.
- [15] G. Degrandi, P. Slavich and F. Zwirner, Nucl. Phys. B611 (2001) 403; A. Brignole, G. Degrandi, P. Slavich and F. Zwirner, Nucl. Phys. B643 (2002) 79; *ibid.* B631 (2002) 195;
- [16] A. Djouadi, J.L. Kneur and G. Moultaka, Comput. Phys. Commun. 176 (2007) 426.
- [17] B. C. Allanach, Comput. Phys. Commun. 143 (2002) 305.
- [18] See for instance, S. Heinemeyer, W. Hollik and G. Weiglein, Phys. Rev. D58 (1998) 091701 and Eur. Phys. J.C9 (1999) 343.
- [19] S. Heinemeyer, W. Hollik and G. Weiglein, Comput. Phys. Commun. 124 (2000) 76.
- [20] P. Kant, R. Harlander, L. Mihaila and M. Steinhauser, JHEP 1008 (2010) 104.
- [21] H.E. Haber and Y. Nir, Phys. Lett. B306 (1993) 327; H.E. Haber, hep-ph/9505240.
- [22] J.F. Gunion, A. Stange, S. Willenbrock et al., hep-ph/9602238.
- [23] E. Boos et al., Phys. Rev. D66 (2002) 055004; E. Boos et al., Phys. Lett. B622 (2005) 311; A. Djouadi and Y. Mambrini, JHEP 0612 (2006) 001; E. Boos, A. Djouadi and A. Nikitenko, Phys. Lett. B578 (2004) 384.

- [24] H. Baer and J. Wells, Phys. Rev. D57 (1998) 4446; W. Loinaz and J.D. Wells, Phys. Lett. B445 (1998) 178; K.S. Babu and C.F. Kolda, Phys. Lett. B451 (1999) 77; M. Carena, S. Mrenna and C.E.M. Wagner, Phys. Rev. D62 (2000) 055008; S. Heinemeyer, W. Hollik and G. Weiglein, Eur. Phys. J. C16 (2000) 139; D. Noth and M. Spira, JHEP 1106 (2011) 084.
- [25] A. Djouadi, Phys. Lett. B435 (1998) 101.
- [26] A. Djouadi, V. Driesen, W. Hollik and J. I. Illana, Eur. Phys. J.C1 (1998) 149.
- [27] A. Arvanitaki and G. Villadoro, JHEP 1202 (2012) 144.
- [28] H. K. Dreiner, J.S. Kim and O. Lebedev, arXiv:1206.3096. See also, A. Djouadi et al., Phys. Lett. B376 (1996) 220; Z. Phys. C70 (1996) 435; Z. Phys. C74 (1997) 93; A. Djouadi, Mod. Phys. Lett. A14 (1999) 359.
- [29] A. Djouadi, J. Kalinowski and M. Spira, Comput. Phys. Commun. 108 (1998) 56.
- [30] D. Albornoz Vasquez, G. Belanger, R. Godbole and A. Pukhov, arXiv:1112.2200 [hep-ph].
- [31] R. Harlander and W. Kilgore, Phys. Rev. D68 (2003) 013001.
- [32] Particle Data Group (K. Nakamura et al.), J. Phys. G37 (2010) 075021.
- [33] A. Arbey, M. Battaglia and F. Mahmoudi, Eur. Phys. J. C72 (2012) 1847.
- [34] M. Muhlleitner, A. Djouadi and Y. Mambrini, Compt. Phys. Com. 168 (2005) 46. It is based on: C. Boehm, A. Djouadi and Y. Mambrini, Phys.Rev. D61 (2000) 095006; A. Djouadi and Y. Mambrini, Phys. Rev. D63 (2001) 115005; A. Djouadi, Y. Mambrini and M. Muhlleitner, Eur. Phys. J. C20 (2001) 563.
- [35] F. Mahmoudi, Comput. Phys. Commun. 178 (2008) 745; F. Mahmoudi, Comput. Phys. Commun. 180 (2009) 1579; A. Arbey and F. Mahmoudi, Comput. Phys. Commun. 181 (2010) 1277.
- [36] M. Spira, Nucl. Instrum. Meth. A389 (1997) 357; hep-ph/9510347. Based on, M. Spira, A. Djouadi, D. Graudenz and P. M. Zerwas, Nucl. Phys. B453 (1995) 17.
- [37] T. Aaltonen *et al.* [CDF Collaboration], Phys. Rev. Lett. 107 (2011) 239903; [Phys. Rev. Lett. 107 (2011) 191801].
- [38] R. Aaij *et al.* [LHCb Collaboration], Phys. Rev. Lett. 108 (2012) 231801.
- [39] S. Chatrchyan *et al.* [CMS Collaboration], JHEP 1204 (2012) 033.
- [40] A. G. Akeroyd, F. Mahmoudi and D. M. Santos, JHEP 1112 (2011) 088; F. Mahmoudi, S. Neshatpour and J. Orloff, arXiv:1205.1845 [hep-ph].
- [41] T. Hurth and F. Mahmoudi, arXiv:1207.0688 [hep-ph].
- [42] E. Aprile *et al.* [XENON100 Collaboration], Phys. Rev. Lett. 107 (2011) 131302.

- [43] E. Komatsu *et al.* [WMAP Collaboration], *Astrophys. J. Suppl.* 192 (2011) 18.
- [44] A. Arbey and F. Mahmoudi, *Phys. Lett. B* 669 (2008) 46; A. Arbey and F. Mahmoudi, *JHEP* 1005 (2010) 051.
- [45] G. Aad *et al.* [ATLAS Collaboration], *Phys. Lett. B* 710 (2012) 67.
- [46] S. Chatrchyan *et al.* [CMS Collaboration], *Phys. Rev. Lett.* 107 (2011) 221804.
- [47] G. Aad *et al.* [ATLAS Collaboration], *Phys. Lett. B* 705 (2011) 174.
- [48] S. Chatrchyan *et al.* [CMS Collaboration], *Phys. Lett. B* 713 (2012) 68.
- [49] G. Aad *et al.* [ATLAS Collaboration], *JHEP* 06 (2012) 039.
- [50] [ATLAS Collaboration], Note ATLAS-CONF-2012-091.
- [51] [CMS Collaboration], Note CMS PAS HIG-2012-015.
- [52] [ATLAS Collaboration], Note ATLAS-CONF-2012-092.
- [53] [CMS Collaboration], Note CMS PAS HIG-2012-016.
- [54] [CMS Collaboration], Note CMS PAS HIG-2012-019.
- [55] [CMS Collaboration], Note CMS PAS HIG-2012-018.
- [56] S. Dittmaier *et al.*, [LHC Higgs cross section working group], arXiv:1101.0593 [hep-ph].
- [57] J. Baglio and A. Djouadi, *JHEP* 1103 (2011) 055.
- [58] [Tevatron Electroweak Working Group and CDF and D0 Collaborations], arXiv:1107.5255 [hep-ex].
- [59] S. Alekhin, A. Djouadi and S. Moch, arXiv:1207.0980 [hep-ph].
- [60] H. Baer, A. Belyaev, T. Krupovnickas and X. Tata, *JHEP* 0402 (2004) 007; *JHEP* 0406 (2004) 061; A. Djouadi, M. Drees and J.-L. Kneur, *Phys. Lett. B* 624 (2005) 60; [hep-ph/0504090].
- [61] A. Arbey, M. Battaglia and F. Mahmoudi, arXiv:1205.2557 [hep-ph].
- [62] R. Benbrik, M. G. Bock, S. Heinemeyer, O. Stal, G. Weiglein and L. Zeune, arXiv:1207.1096 [hep-ph].